Pergamon

Acta Materialia 50 (2002) 421–440

Acta MATERIALIA

www.elsevier.com/locate/actamat

Theory of orientation gradients in plastically strained crystals

D. Raabe [a,*], Z. Zhao [a], S.-J. Park [b], F. Roters [a]

[a] *Max-Planck-Institut für Eisenforschung, Max-Planck-Str. 1, 40237 Düsseldorf, Germany*
[b] *Department of Materials Science and Engineering, Seoul National University, Seoul, South Korea*

Received 13 December 2000; received in revised form 14 August 2001; accepted 14 August 2001

Abstract

We suggest a theory of in-grain orientation gradients in plastically strained metals. It is an approach to explain why initially uniformly oriented crystals can—under gradient-free external loadings—build up in-grain orientation gradients during plastic deformation and how this phenomenon depends on intrinsic factors (crystal orientation) and extrinsic factors (neighbor grains).

The intrinsic origin (orientation dependence) of in-grain orientation gradients is investigated by quantifying the change in crystal reorientation upon small changes in initial orientation. This part of the approach is formulated by applying a divergence operator to reorientation rate vector fields (in the present paper calculated by using strain-rate homogenization Taylor–Bishop–Hill theory). The obtained scalar divergence function (but not the reorientation vector field itself) quantifies the kinematic stability of grains under homogeneous boundary conditions as a function of their orientation. Positive divergence (source in the reorientation rate vector field) characterizes orientations with diverging non-zero reorientation rates which are kinematically unstable and prone to build up orientation gradients. Zero divergence indicates orientations with reorientation rate identity with the surrounding orientations which are not prone to build up orientation gradients. Negative divergence (sink in the reorientation rate vector field) characterizes orientations with converging non-zero reorientation rates which are kinematically stable and not prone to build up orientation gradients. Corresponding results obtained by use of a crystal plasticity finite element formulation are in good agreement with the reorientation field divergence function derived by homogenization theory.

The extrinsic origin of in-grain orientation gradients (influence of grain–neighbor interaction) is addressed using a crystal plasticity finite element bicrystal model. The simulations show that a significant dependence of orientation gradients on the neighbor crystals occurs for grains with high positive divergence. The build-up of orientation gradients in grains with close to zero or negative divergence is in body centered cubic crystals less sensitive to the presence of neighbor orientations than in face centered cubic crystals (Goss and cube orientation). © 2002 Published by Elsevier Science Ltd on behalf of Acta Materialia Inc.

Keywords: Texture; Theory & modeling; Structural behaviour; Mesostructure

* Corresponding author. Tel.: +49-211-6792-340/278; fax: +49-211-6792-333.
E-mail address: raabe@mpie.de (D. Raabe).

1359-6454/02/$22.00 © 2002 Published by Elsevier Science Ltd on behalf of Acta Materialia Inc.
PII: S1359-6454(01)00323-8

1. Introduction

1.1. Phenomenology and terminology of orientation gradients

Plastic deformation of poly- and single crystals can lead to individual orientation changes of the grains and, as a consequence, to the development of deformation textures. However, initially uniformly orientated crystals do often not rotate as units but subdivide into portions with a range of different orientations. We refer to this phenomenon, which was already in 1940 observed and discussed by Barrett and Levenson [1], to the formation of orientation gradients, meaning spatial continuous or discontinuous variations of crystal orientation within the original grain borders.

Orientation gradients do not only form in the trivial case of externally imposed strain gradients (e.g. bulk torsion or rolling operations with non-zero friction) but also under gradient-free external loadings. They are in the literature also referred to as localized orientation gradients [2], grain fragmentation [3], deformation banding [4–6] orientation splitting [7], grain subdivision [4,8], or lattice curvature [8–11].

Beaudoin et al. [2], Raabe [3], Leffers [4], and Lee et al. [5,6] provided theoretical approaches to explain the formation of a non-uniform orientation spread within a grain. Using many elements per grain Beaudoin et al. [2] observed in their 3D crystal plasticity simulations heterogeneous deformations within individual grains which lead to the development of domains which were separated by boundaries of high misorientation. Similar investigations using crystal plasticity finite element methods were also conducted by other authors (e.g. [1,12–21]). Raabe [3], Leffers [4], and Lee et al. [5,6] gave arguments for the formation of orientation gradients on the basis of modified homogenization models.

The term lattice curvature was typically used by authors who underlined the mechanical aspects of continuous in-grain orientation gradients [8–10], mainly referring to the formation of geometrically necessary dislocations.

Quantitative experimental work on this subject was essentially conducted using orientation imaging techniques via analysis of Kikuchi diffraction patterns in the scanning electron microscope (SEM) (e.g. [22–38]) and in the transmission electron microscope (TEM) (e.g. [37–41] [42–48]). Earlier experimental work about orientation gradients was based on analysis of X-ray Bragg diffraction pole figures, Kossel diffraction patterns, electron channeling patterns, etch pits, and orientation sensitive etching methods.[1]

The above described phenomena can occur in single crystals as well as in grains of polycrystals. From the quoted literature some common features of in-grain orientation gradient phenomena can be identified: Orientation gradients were found

1. to occur under homogeneous boundary conditions, i.e. they take place even if no gradients are exerted by external loading (the internal load is usually less well known) (e.g. [2,6,11,23]);
2. to depend on the strain path (e.g. [11]);
3. in many cases to depend on the initial orientation and on the orientation path of the strained crystal (e.g. [3,11,19,24,30,31,33]);
4. in many cases to depend on the neighbor grains (e.g. [1,2,12–19]);
5. to be closely connected with a change in glide system activity in the different in-grain portions with different orientations (e.g. [11,24,41,47,48]) (such in-grain domains of different orientation have in these works been referred to as *differently deforming regions*);
6. in many cases to occur already at low strains and build up further throughout deformation (e.g. [1,3,7,24]);
7. to undergo continued refinement in the spatial scale of subdivision with increasing total strain and to occur at different spatial scales within the same crystal (e.g. [12,24,30–32]).

In order to avoid confusion we will use the expression *orientation gradient* (here always meaning *in-grain* orientation gradient) as a rep-

[1] Since this is no overview paper on experimental methods, we quote only a selected set of papers and refer the interested reader to the RISØ-overview of Hughes [47].

resentative term for the various phenomena listed above in the ensuing sections of the paper.

1.2. Aims of an orientation gradient theory

Besides the basic scientific challenge to elucidate the origin of orientation gradients, five main practical reasons can be given for the formulation of an orientation gradient theory. First, due to the complexity of existing results and details observed so far theory is required to better understand and structure the underlying principles of orientation gradients. Second, the key idea of our approach, namely the use of the reorientation rate vector field divergence as an intrinsic measure of orientation gradients can be formulated as a concise scalar function in orientation space using for instance spherical harmonics. Third, our formulation is tractable for subsequent integration into other frameworks dealing with the orientation dependence of recrystallization or strain hardening phenomena. Fourth, theoretical concepts help to separate important from less important microstructural information in the context of orientation gradients. Fifth, complete experimental instead of theoretical characterization of in-grain orientation gradient phenomena throughout orientation space is not possible due to the huge number of crystal orientations and boundary conditions to be considered.

1.3. Basic theoretical approach

The present work aims at explaining why uniform crystals can build up orientation gradients during plastic deformation and how this phenomenon depends on crystal orientation (*intrinsic* dependence) and on the interaction with neighbor grains (*extrinsic* dependence). The intrinsic origin of orientation gradients is investigated on the basis of the geometrical stability of grains with respect to small changes in starting orientation. The orientation dependence of orientation gradients is in the intrinsic approach, i.e. without consideration of neighbor interaction, formulated by applying a divergence operator to reorientation rate vector fields in orientation space. This scalar divergence function then quantifies stability of grains under homogeneous boundary conditions as a function of orientation and strain state. Extrinsic reasons for orientation gradients are addressed by calculating the influence of grain–neighbor interaction directly using a crystal plasticity finite element approach.

1.4. Plan of the paper

The plan of the paper is as follows: In Section 2 we introduce the reorientation field divergence as a scalar function in Euler space for quantifying the intrinsic origin of orientation gradients and formulate it for fcc and bcc crystals for the plane strain case. In Section 3 we check the consistency of these predictions by use of crystal plasticity finite element simulations. In Section 4 we investigate the influence of neighborhood on the formation of orientation gradients using a crystal plasticity finite element bicrystal model. Section 5 provides a discussion of the predictions, compares the findings with experimental data from the literature, and explains differences found between the fcc and the bcc structure.

2. Divergence of crystal reorientation fields as intrinsic measure for orientation gradients

2.1. Concept and calculation method

The theoretical approach we suggest in this paper for the explanation of the formation of in-grain orientation gradients under homogeneous external boundary conditions is based on strain rate homogenization modeling and on crystal plasticity finite element modeling. It aims at explaining why initially uniformly oriented crystals can under homogeneous boundary conditions form in-grain orientation gradients during plastic straining and how this phenomenon depends on crystal orientation (*intrinsic* dependence) and on grain–neighbor interaction (*extrinsic* dependence). In contrast to some of the above quoted works the present investigation does not make any predictions about the spatial arrangement, size, or shape of in-grain orientation gradients but provides a more general geometrical approach for calculating what the potential tendency of a particular grain is to form orientation gradients within its original

borders as a function of its initial orientation, its neighbor grains, and the strain state.

The intrinsic origin of orientation gradients is investigated on the basis of the kinematic stability of grains with respect to small changes in starting orientation. This follows a suggestion of Kocks [49] who stated that orientation gradient effects may proceed from a variation in slip system activation throughout a grain entailing microscopic initial variation in slip and hence in the plastic rotation leading to local domains with different orientation. We will extent this approach and show that the tendency to build up orientation gradients can be formulated in terms of the *orientation dependence* of such in-grain variations in slip system selection and the resulting in-grain spread of the reorientation rate. A consequence of this model is that one can quantify the orientation dependence of the phenomenon by calculating the dependence of reorientation rate upon tiny changes in the initial *host* orientation.

It will be shown that it is a strong function of the grain orientation itself whether such initial variations entail in-grain orientation gradients during plastic straining or not. As was found earlier and as will be shown below the reorientation rate vector *itself* is not an adequate measure of future orientation gradients.

The orientation dependence of in-grain orientation gradients is in the intrinsic approach, i.e. without consideration of neighbor interaction, formulated by applying a divergence operator to reorientation rate vector fields in orientation space. Such fields are generated by mapping the reorientation rate vectors obtained (in the present case) from strain-rate homogenization theory for each orientation throughout orientation space (see e.g. [11,49–51]). This scalar divergence function then quantifies kinematic stability of grains under homogeneous boundary conditions as a function of orientation and strain state.

It is obvious that such a divergence analysis of reorientation paths is a general approach for quantifying orientational instabilities. It should be noted though that the analysis of orientation stability is not necessarily a non-linear problem, since many homogenization models are linear. However, the here suggested divergence approach for the analysis of orientational stability is generally independent on the underlying deformation model or experiment. Its starting point is simply a theoretically derived or experimentally observed reorientation field in orientation space (not in real space).

Fig. 1 describes the principle of our approach (intrinsic case). The size of the different grain regions is purely schematical. Fig. 1(a) shows a grain in the initial state with some small initial orientation variation and after straining with a larger orientation variation. This is a case where the initial orientation variation becomes stronger during straining, due to different slip system activation in the different regions. This is a case where reorientation vectors of different regions in the same grain are non-zero and point in opposite directions (arrows). Mathematically this corresponds to a positive divergence of the reorientation field (source in the reorientation vector field) characterizing kinematically unstable orientations which have an intrinsic tendency to build up orientation gradients.

Fig. 1(b) shows a case where reorientation vectors of different regions in the same grain are non-zero and identical. This means the entire grain rotates homogeneously with the same reorientation vector. In this case the initial orientation fluctuation remains unchanged, but the bulk grain undergoes bulk reorientation. Mathematically this corresponds to zero divergence of the reorientation field (reorientation identity of the different orientation segments) characterizing orientations which do not have an intrinsic tendency to build up orientation gradients.

Fig. 1(c) shows a case where reorientation vectors of different regions in the same grain are non-zero and point towards each other, or more general, towards the same stable orientation. In this case the initial orientation fluctuation becomes smaller. Mathematically this corresponds to negative divergence of the reorientation field (sink in the reorientation vector field) indicating orientations which do not have an intrinsic tendency to build up orientation gradients.

For obtaining an intrinsic function of grain fragmentation which depends solely on crystal orientation and which is independent of neighbor grain interaction we calculated reorientation fields by

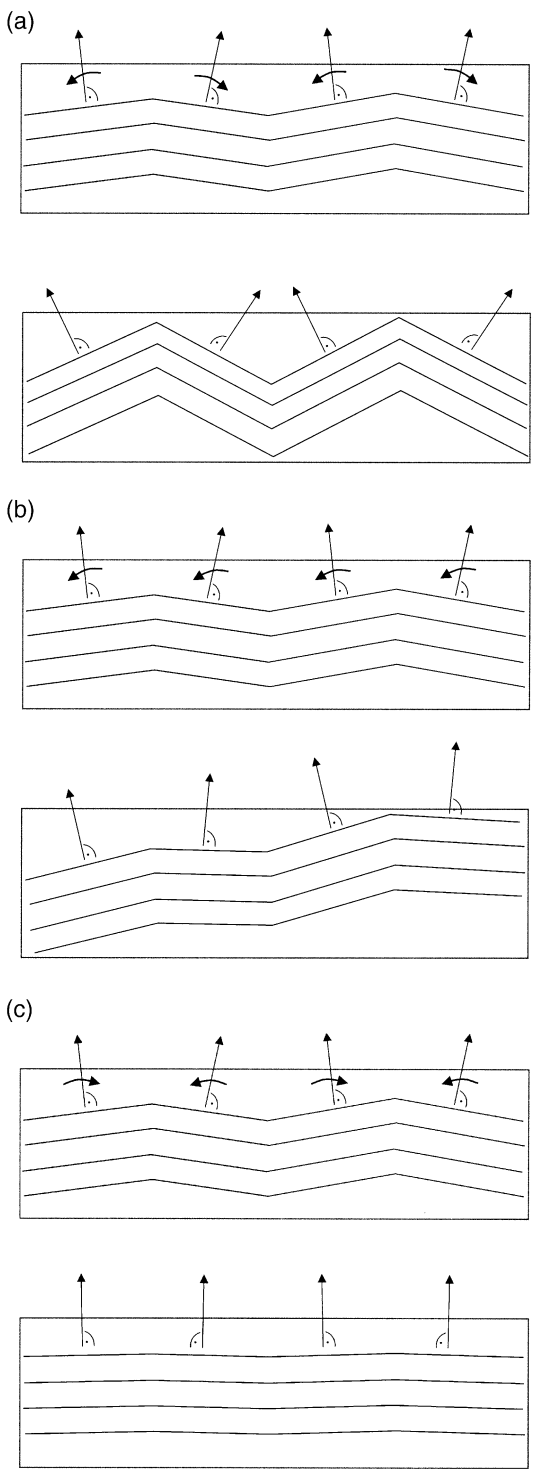

Taylor–Bishop–Hill strain-rate homogenization theory. Calculations were conducted for body centered cubic (bcc) crystal structure with 12 {110}<1̲11> slip systems and 48 slip systems (12×{11̲0}<111>, 12× {112̲}<111>, 24× {123̲}<111>) as well as for face centered cubic (fcc) crystal structure with 12× {11̲1}<110> slip systems and 18 slip systems (12× {11̲1}<110>, 6× {11̲0}<110>), exerting homogeneous external plane strain conditions with relaxation of longitudinal and transverse shear constraints at the grain level (pancake model) (see overviews in [55–57]). Finally we applied a divergence operator to the obtained reorientation vector field. The resulting scalar divergence function was developed in the form of spherical harmonics using a series expansion degree of 34 and then plotted in orientation space.

Since the approach suggested in this paper essentially takes a geometrical view at the development of crystal orientations it is only capable of addressing observations (1)–(6). Observations (7) cannot be explained in the present framework since this would require to include dislocation dynamics

Fig. 1. (a) Grain in the initial state with some small initial orientation variation and after straining with a larger orientation variation. This is a case where the initial orientation variation becomes stronger during straining, due to different slip system activation in the different regions. This is a case where reorientation vectors of different regions in the same grain are non-zero and point in opposite directions (arrows). Mathematically this corresponds to a positive divergence of the reorientation field (source in the reorientation vector field) indicating orientations which have a tendency to form orientation gradients. (b) Case where reorientation vectors of different regions in the same grain are non-zero and identical. The entire grain rotates homogeneously with the same reorientation vector. In this case the initial orientation fluctuation remains unchanged, but the grain undergoes bulk reorientation. Mathematically this corresponds to zero divergence of the reorientation field (reorientation identity with the surrounding orientations) indicating orientations which do not have a tendency to form orientation gradients. (c) Case where reorientation vectors of different regions in the same grain are non-zero and point towards each other, or more general, towards the same stable orientation. In this case the initial orientation fluctuation becomes smaller. Mathematically this corresponds to negative divergence of the reorientation field (sink in the reorientation vector field) indicating orientations which do not have a tendency to form orientation gradients.

based effects [9,52–54] which are not part of this investigation.[2] On the other hand it is likely that, due to the dominance of the reorientation field for the formation of orientation gradients [11,50,51], explicit incorporation of dislocation dynamics effects would lead to an overall damping force, i.e. to slower rotations, rather than to entirely different results. In other words, this paper concentrates on the *kinematic origin* of orientation gradients, i.e. on the role of changes in slip system selection and the resulting reorientation changes as a function of orientation.

2.2. Results for body centered cubic crystal structure (intrinsic, reorientation field divergence)

Fig. 2 shows the reorientation field divergence of a bcc polycrystal with 12 slip systems, derived by using the pancake model. The figure is in the form of φ_1=constant sections in Euler-space to show the divergence along relevant plane strain deformation and shear texture fibers and components.[3] The intensity lines show areas with positive divergence above +1. The diagram shows high divergence around the rotated cube ($\{001\}\langle 110\rangle$, $\varphi_1 = 0°$, $\phi = 0°$, $\varphi_2 = 45°$) and the Goss ($\{011\}\langle 100\rangle$, $\varphi_1 = 0°$, $\phi = 45°$, $\varphi_2 = 0°$) texture components as well as along the ζ-fiber. This is only in part in accord with experimental experience. Whilst orientations around Goss and

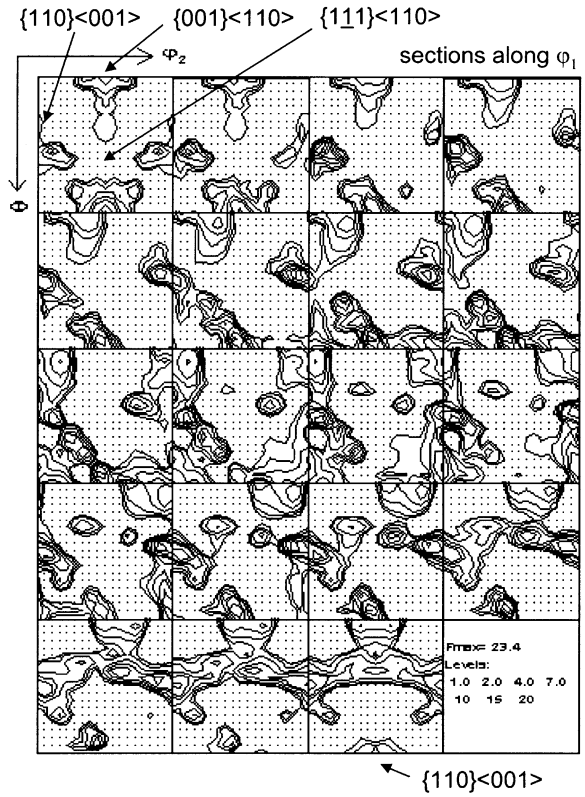

Fig. 2. Reorientation rate vector field divergence of a bcc polycrystal with 12 slip systems; pancake model; φ_1=constant sections in Euler space; intensity lines show areas with divergence above 1.

the ζ-fiber are indeed known to form strong orientation gradients under plane strain conditions, the rotated cube orientation $\{001\}\langle 110\rangle$ is known as a very stable component without building up pronounced in-grain orientation gradients during plane strain deformation (see experiments in [30,31,33,58]). Section 5 will provide a more detailed comparison with experimental data.

Fig. 3(a) shows the reorientation field divergence for 48 slip systems (bcc, pancake model). It reveals high divergence around the Goss component and an absolute maximum at the RZ_{bcc} component ($\varphi_1 = 34°$, $\phi = 84°$, $\varphi_2 = 45°$). Fig. 3(b) shows in the form of a $\varphi_2 = 45°$-section some details of the divergence between 0.1 and 1. It can be seen that some orientations around the γ-fiber and on the α-fiber reveal small positive divergence.

[2] Attempts were made to calculate microtextures from discrete dislocation dynamics [54]. However, such approaches are computationally too time-consuming for formulating a theory of orientation gradients.

[3] For bcc materials these are the α_{bcc}-fiber (fiber axis $\langle 110\rangle$ parallel to the rolling direction including major components $\{001\}\langle 110\rangle$, $\{1\underline{1}2\}\langle 110\rangle$, and $\{1\underline{1}1\}\langle 110\rangle$), γ-fiber (fiber axis $\langle 111\rangle$ parallel to the normal direction including major components $\{111\}\langle 1\underline{1}0\rangle$ and $\{11\underline{1}\}\langle 11\underline{2}\rangle$), η-fiber (fiber axis $\langle 001\rangle$ parallel to the rolling direction including major components $\{001\}\langle 100\rangle$ and $\{011\}\langle 100\rangle$), ζ-fiber (fiber axis $\langle 011\rangle$ parallel to the normal direction including major components $\{011\}\langle 100\rangle$, $\{0\underline{1}1\}\langle 211\rangle$, $\{0\underline{1}1\}\langle 111\rangle$, and $\{0\underline{1}1\}\langle 011\rangle$), ϵ-fiber (fiber axis $\langle 011\rangle$ parallel to the transverse direction including major components $\{001\}\langle 110\rangle$, $\{11\underline{2}\}\langle 111\rangle$, $\{111\}\langle 11\underline{2}\rangle$, and $\{011\}\langle 100\rangle$), and θ-fiber (fiber axis $\langle 001\rangle$ parallel to the normal direction including major components $\{001\}\langle 100\rangle$ and $\{001\}\langle 110\rangle$).

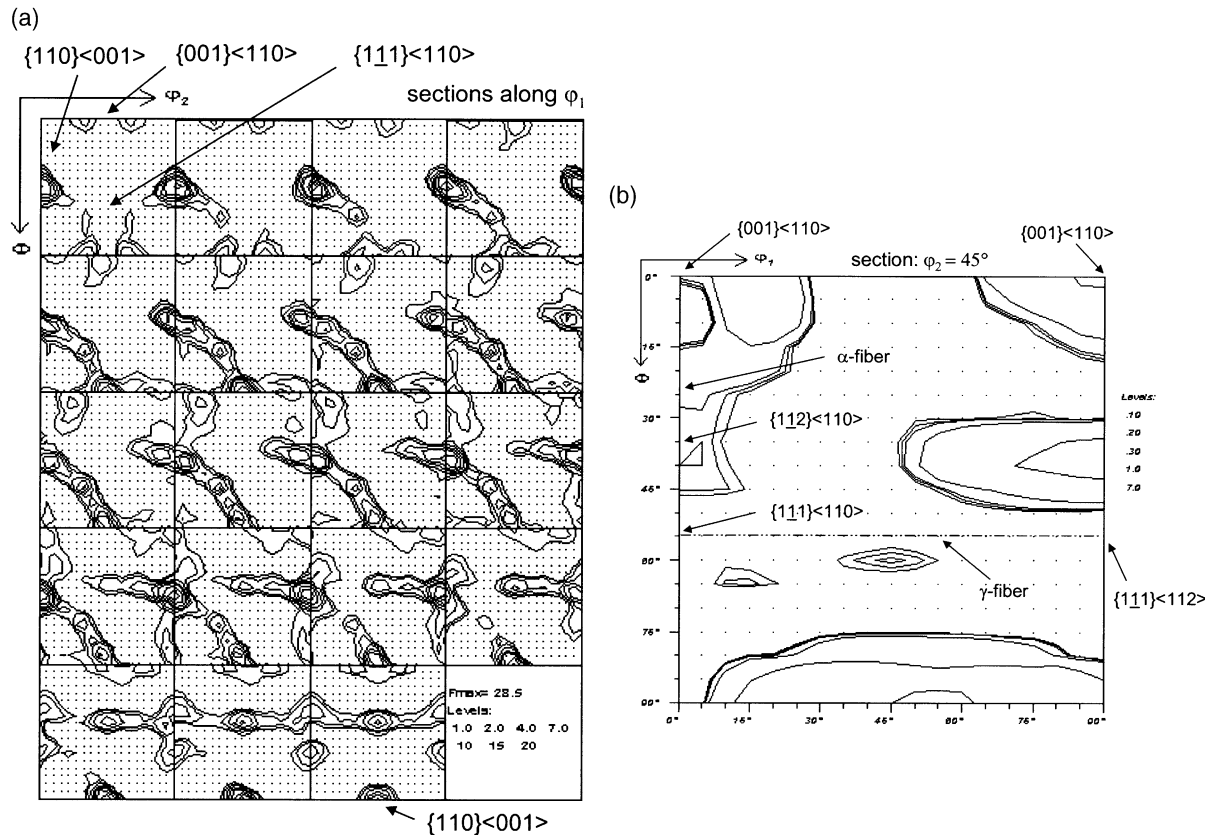

Fig. 3. (a) Reorientation rate vector field divergence of a bcc polycrystal with 48 slip systems; pancake model; φ_1=constant sections in Euler space; intensity lines show areas with divergence above +1. (b) Details of the divergence function shown in (a) between 0.1 and 1.

2.3. Results for face centered cubic crystal structure (intrinsic, reorientation field divergence)

Fig. 4 shows the reorientation field divergence of a fcc polycrystal with 12 slip systems, calculated by using the pancake model. The figure is in the form of φ_2=constant sections to show relevant components of typical fcc plane strain deformation and shear textures.[4]

The results show strong divergence close to the {001}<110> component. This is equivalent to the divergence observed around the Goss component for the bcc structure because of the 90° rotation relationship about the transverse direction between the fcc and the primary 12 bcc slip systems. Significant divergence appears in the vicinity of the Brass component ({110}<1$\bar{1}$2>) and towards higher angles on the α_{fcc}-fiber. According to the predictions the Goss and the cube orientation should reveal a relatively weak intrinsic tendency to build up orientation gradients. This is in contradiction to experimental observations. In the following sections we will show, that these deviations are essentially due to the influence of the neighbor grains which are not included in this section. Calculations on the basis of 18 slip systems reveal

[4] For fcc materials these are the α_{fcc}-fiber (fiber axis <011> parallel to the normal direction including major components {011}<100>, {011}<2$\bar{1}$1>, {011}<1$\bar{1}$1>, and {011}<0$\bar{1}$1>) and the β-skeleton line (less symmetric fiber including major components {211}<111> (Cu-component), ~{123}<634> (S-component) and {011}<211> (Brass-component)).

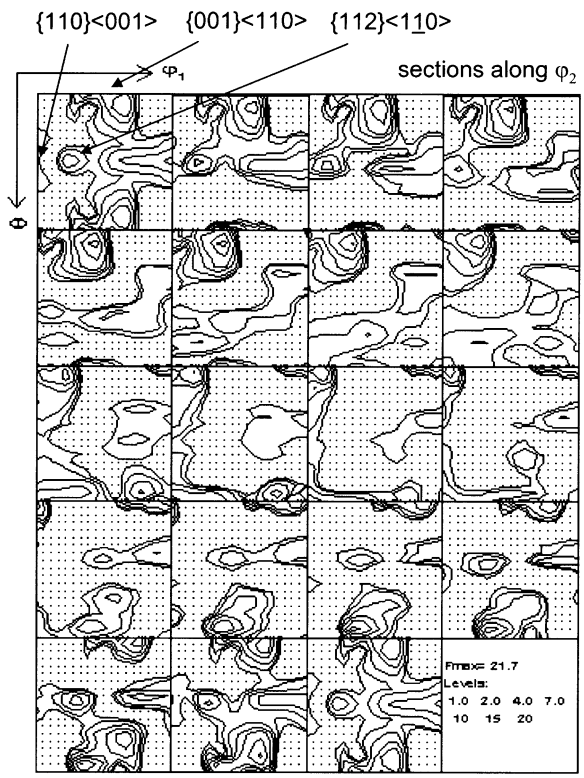

Fig. 4. Reorientation rate vector field divergence of a fcc polycrystal with 12 slip systems; pancake model; φ_2=constant sections in Euler space; intensity lines show areas with divergence above +1.

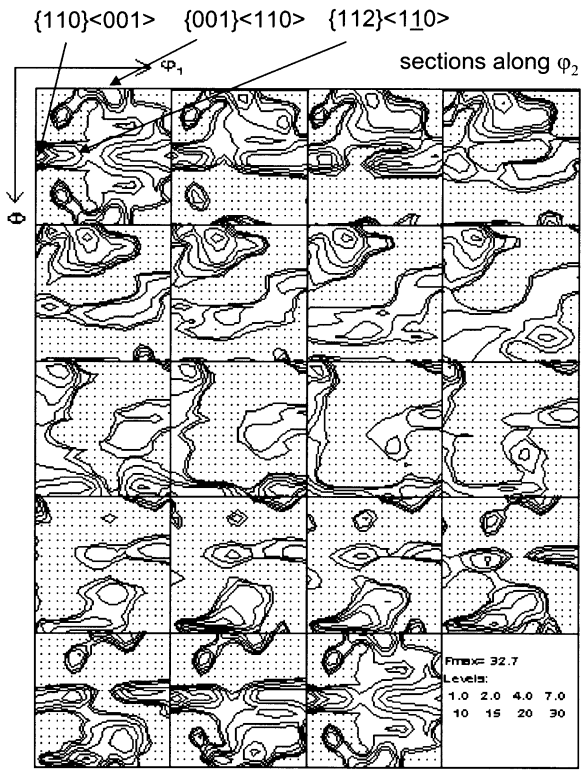

Fig. 5. Reorientation rate vector field divergence of a fcc polycrystal with 18 slip systems; pancake model; φ_2=constant sections in Euler space; intensity lines show areas with divergence above +1.

similar divergence behavior (Fig. 5). The maximum on the α_{fcc}-fiber is shifted from the Brass towards the Goss component.

3. Verification of the reorientation field divergence theory using a crystal plasticity finite element method

3.1. Concept and calculation method

The results obtained form the divergence calculations presented in the preceding section are influenced by the homogenization model used for the calculation of the reorientation fields. Various approaches can be used for the calculation of the reorientation field, for instance crystal plasticity finite element, Taylor–Bishop–Hill, or self-consistent models.

This section presents crystal plasticity finite element calculations showing predictions of orientation gradients of selected single crystal orientations under external (not necessarily internal) plane strain boundary conditions. The results are compared with the predictions made in the previous section. In order to simulate external plane strain conditions the free surface of the crystals was constrained to preserve orthorhombic symmetry during plastic straining.

Mesh configuration was conducted via ABAQUS/CAE [59] using a 3-dimensional linear element type with eight nodes and eight integration points. The total number of elements was 512 (8×8×8). An implicit crystal plasticity procedure proposed by Kalidindi et al. [60] was implemented

and used for the time integration of the constitutive equations. Calculations were carried out using the finite element program ABAQUS in conjunction with the user defined material subroutine UMAT [59]. Simulations were based on 48 slip systems (12× {110}<111>, 12× {112}<111>, 24× {123}<111>) in case of bcc crystals and on 12 {111}<110> slip systems in case of fcc crystals. For selected bcc and fcc grain orientations plane strain compression to 50% thickness reduction was simulated (thickness reduction is given as $\Delta d/d_0$, where d is the thickness).

3.2. Results for body centered cubic crystal structure (intrinsic, FEM)

Fig. 6(a) shows the accumulated misorientations in gray scale coding (with light values indicating large misorientations) for a bcc grain with initial rotated cube orientation, {001}<110>, after 50% plane strain deformation. The projected orientation distribution is given in the form of {111} pole figures. The open squares show the initial orientation (which was the same at all integration points). The black dots show the orientations of all integration points after deformation. It is remarkable, that neither bulk rotation nor orientation gradients occur. This behavior corresponds to the case described in Fig. 1(c). The prediction is in very good accord with the reorientation divergence model using 48 slip systems [Fig. 3(a,b)].

Fig. 6(b) shows the results for the inverse Brass component ({112}<1$\underline{1}$0>, $\varphi_1 = 0°$, $\phi = 35°$, $\varphi_2 = 45°$). It can be seen that the initially uniform grain has split up into two different orientation

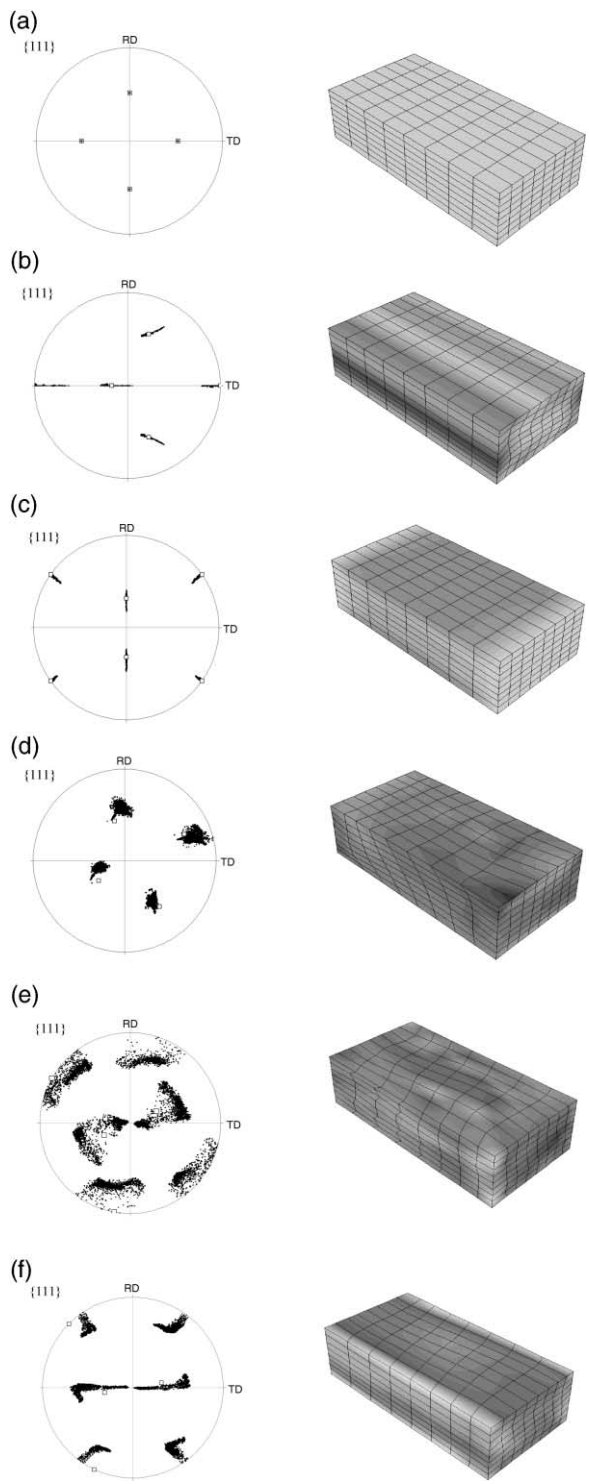

Fig. 6. Accumulated misorientations in gray scale coding (light values indicate large misorientations) for a bcc grain (48 slip systems) after 50% plane strain deformation. The texture is given in the form of {111} pole figures. The open square shows the initial orientation (which was the same at all integration points) and the black dots show the orientations after deformation. The starting orientations were (a) 45° rotated cube orientation ($\varphi_1 = 0°$, $\phi = 0°$, $\varphi_2 = 45°$); (b) inverse Brass orientation ($\varphi_1 = 0°$, $\phi = 35°$, $\varphi_2 = 45°$); (c) Goss orientation ($\varphi_1 = 0°$, $\phi = 45°$, $\varphi_2 = 0°$); (d) less symmetric orientation ($\varphi_1 = 0°$, $\phi = 18°$, $\varphi_2 = 73°$); (e) RZ_{bcc} orientation ($\varphi_1 = 34°$, $\phi = 84°$, $\varphi_2 = 45°$); (f) 90° rotated Goss orientation ($\varphi_1 = 0°$, $\phi = 90°$, $\varphi_2 = 45°$).

branches, related to each other by a rotation about the longitudinal direction, corresponding to a crystal <110> axis. The mutually misoriented volume portions are connected by orientational transition bands. This behavior corresponds to the case described by Fig. 1(a). The reorientation divergence model also predicts a positive though weak divergence value matching this result [see Fig. 3(b) around $\phi = 35°$, $\varphi_1 = 0°$).

Fig. 6(c) shows the results for the Goss orientation. The grain has split into two different sharp orientation branches, related to each other by a rotation about the transverse direction <0$\underline{1}$1>. As in the previous case a transition zone mediates between the orientation fragments. This results is in excellent accord with the prediction of the reorientation divergence model, which revealed a maximum divergence close to the Goss component [Fig. 3(a)].

Fig. 6(d) shows the results for the less symmetric orientation $\varphi_1 = 0°$, $\phi = 18°$, $\varphi_2 = 73°$, which was chosen because it is known to be unstable and tends to rotate towards the α_{bcc}-fiber under plane strain conditions. It can be seen that the crystal, though building up minor orientation gradients, nearly rotates in one piece and does not split into different orientation branches with dissimilar orientation paths. This behavior corresponds to the case described by Fig. 1(b). The result is in excellent accord with the reorientation divergence model, which predicts a very small value for this component.

Fig. 6(e) shows the results for the RZ_{bcc} orientation, $\varphi_1 = 34°$, $\phi = 84°$, $\varphi_2 = 45°$, which was chosen because it was identified as the absolute maximum in the reorientation divergence model (Fig. 3). The pole figure obtained by the crystal plasticity finite element simulation confirms a very strong tendency of the originally uniformly oriented grain to form orientation gradients. The pole figure shows a scattered array of orientation fragments after straining, which reveal accumulated orientation changes of up to 45° from their initial orientation prior to deformation.

Fig. 6(f) shows the results for the rotated Goss orientation ({110}<110>, $\varphi_1 = 0°$, $\phi = 90°$, $\varphi_2 = 45°$), which splits strongly during straining. This in excellent accord with the reorientation field divergence model, which shows a local maximum close to the rotated Goss orientation. Since the component is itself unstable under plane strain conditions, it rotates into this maximum and then starts to split up and form orientation gradients as predicted in the previous section.

3.3. Results for face centered cubic crystal structure (intrinsic, FEM)

Fig. 7(a) shows the accumulated misorientations in gray scale coding (using light values for large misorientations) for a fcc grain with initial Goss orientation after 50% reduction in thickness. The orientation distribution is given in the form of {111} pole figures. The open squares show the initial orientation (which was the same at all integration points). The black dots show the orientations of all integration points after deformation. For the Goss orientation neither bulk rotation of the entire crystal nor in-grain orientation gradients have occurred during plastic straining. This behavior corresponds to Fig. 1(c). It is in very good accord with the reorientation divergence model using 12 slip systems (Fig. 4). The Goss orientation in fcc crystals with 12 slip systems is under plane strain conditions kinematically similar to the rotated cube orientation in bcc crystals with 48 slip systems [Fig. 6(a)]. The similarity is due to the 90° transverse rotation relationship which exists between the two texture components on the one hand and the 12 fcc {1$\underline{1}$0}<111> slip systems and the 12 primary bcc {111}<1$\underline{1}$0> slip systems on the other hand [61]. As will be discussed in the next section the stability of the bcc rotated cube orientation and of the fcc Goss orientation are influenced differently by grain neighbor interaction. It turns out that the fcc Goss orientation is strongly affected by neighbor grains.

Fig. 7(b) shows the results for the Brass component ({110}<1$\underline{1}$2>, $\varphi_1 = 35°$, $\phi = 45°$, $\varphi_2 = 0°$). It can be seen that the initially uniform grain has changed its overall orientation and at the same time built up strong orientation gradients inside its borders. The reorientation divergence model shown in Fig. 4 is in excellent accord with this observation since it predicts a pronounced positive divergence matching the finite element result (see Fig. 4

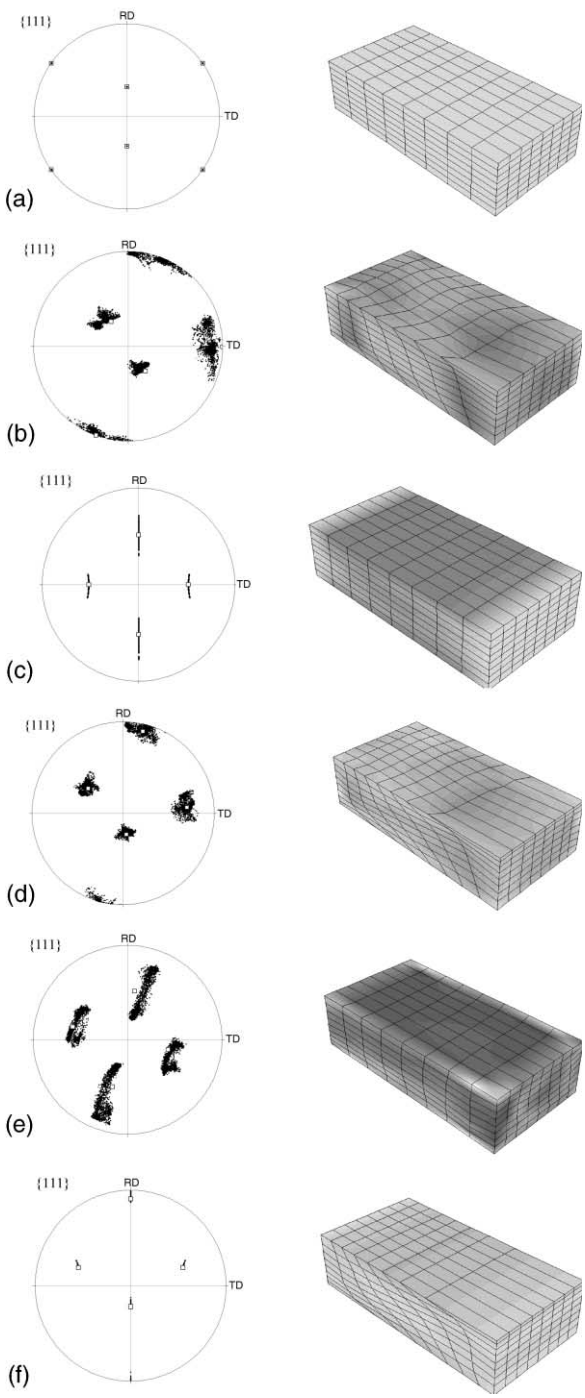

between $\varphi_1 = 30°$ and 35° at $\phi = 45°$ in the $\varphi_2 = 0°$ section).

Fig. 7(c) shows the results for the 45° rotated cube orientation. It can be observed that the grain has formed pronounced orientation gradients resulting in two different orientation branches, related to each other by a $<0\underline{1}1>$ crystal rotation axis parallel to the transverse direction. A transition zone preserving the original bulk orientation remains between the orientation fragments [11]. This results is in very good accord with the prediction of the reorientation divergence model, which showed a pronounced positive value of the divergence at the rotated cube orientation in the first section of Fig. 4.

Fig. 7(d) shows the result for the less symmetric S orientation ($\{123\}<6\underline{3}4>$, $\varphi_1 = 60°$, $\phi = 32°$, $\varphi_2 = 65°$) which was already well investigated using crystal plasticity simulations by Beaudoin et al. [2]. It can be seen that the crystal, though undergoing substantial formation of orientation gradients, rotates as an entity and does not break up into completely different orientation branches with dissimilar orientation paths. This behavior corresponds to the case described by Fig. 1(b). The result corresponds very well to the reorientation divergence model which predicts a rather small value for this component.

Fig. 7(e) shows the results for the RZ_{fcc} orientation ($\varphi_1 = 32°$, $\phi = 85°$, $\varphi_2 = 85°$), which was chosen because it was identified as the absolute maximum in the reorientation divergence model for an fcc material with 12 slip systems (Fig. 4). The pole figure obtained by the crystal plasticity finite element simulation indeed confirms a very strong tendency to build up strong orientation

Fig. 7. Accumulated misorientations in gray scale coding (light values indicate large misorientations) for a fcc grain (12 slip systems) after 50% plane strain deformation. The texture is given in the form of {111} pole figures. The open square shows the initial orientation (which was the same at all integration points) and the black dots show the orientations after deformation. The starting orientations were (a) Goss orientation ($\varphi_1 = 0°$, $\phi = 45°$, $\varphi_2 = 0°$); (b) Brass orientation ($\varphi_1 = 35°$, $\phi = 45°$, $\varphi_2 = 0°$); (c) 45° rotated cube orientation ($\varphi_1 = 45°$, $\phi = 0°$, $\varphi_2 = 0°$); (d) S orientation ($\varphi_1 = 60°$, $\phi = 32°$, $\varphi_2 = 65°$); (e) RZ_{fcc} orientation ($\varphi_1 = 32°$, $\phi = 85°$, $\varphi_2 = 85°$); (f) Copper orientation ($\varphi_1 = 90°$, $\phi = 35°$, $\varphi_2 = 45°$).

gradients within the originally uniformly oriented grain. Some of the orientation fragments reveal accumulated orientation changes which are much larger than in all other investigated fcc crystals.

Fig. 7(f) shows the results for the Copper orientation ({112}<111>, $\varphi_1 = 90°$, $\phi = 35°$, $\varphi_2 = 45°$) which forms only weak orientation gradients during straining. This in good accord with the reorientation divergence model (Fig. 4).

4. Influence of neighbor grains on the tendency to form in-grain orientation gradients

4.1. Concept and calculation method

This section is concerned with the simulation of the influence of the plastic interaction between a grain and its neighbor grains on its tendency to form orientation gradients. This *extrinsic* effect on orientation gradients is investigated by exposing different bicrystal arrangements to external plane strain loading using the crystal plasticity finite element method sketched above. Boundary conditions were assigned to the free surface to constrain the entire assembly to an orthorhombic shape in the course of plastic straining (Fig. 8). Mesh configuration was carried out using ABAQUS/CAE [59]. The element number in the 3D model was 512 (8×8×8) elements with 64 of them (4×4×4) in the center part. A 3D solid linear element type with eight nodes and eight integration points was employed. An implicit procedure proposed by Kalidindi et al. [60] was used as constitutive crystal plasticity model. The scheme was implemented in the finite element program ABAQUS via the material subroutine UMAT [59].

Different crystal orientations, characterized by different reorientation rate and reorientation divergence, were assigned to the center and surrounding crystal, respectively. The compound was then exposed to 50% thickness reduction, like the single crystals discussed above.

4.2. Results for body centered cubic crystal structure (extrinsic, FEM)

Fig. 9(a) shows an example of a deformed bicrystal consisting of two grains with bcc crystal

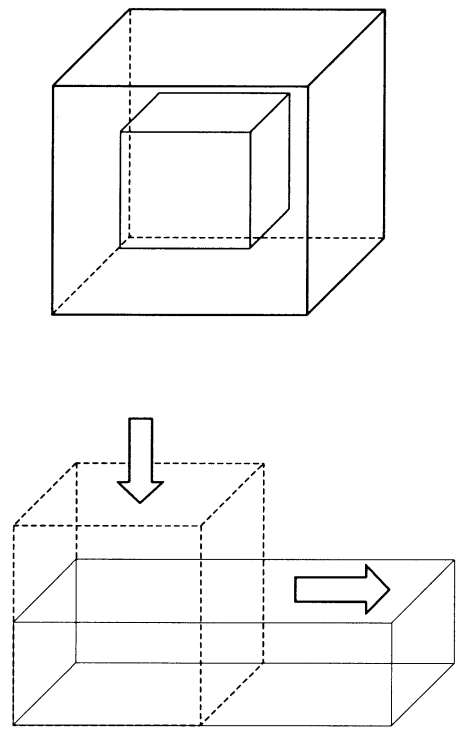

Fig. 8. The bicrystal set-up and displacement conditions used in the crystal plasticity finite element simulations. To simulate the influence of plastic neighbor interaction among the grains, i.e. the extrinsic component of grain fragmentation, different bicrystal arrangements were investigated under external plane strain loading. The free surface was constrained to preserve orthorhombic symmetry.

structure with 12× {1$\underline{1}$0}<111>, 12× {11$\underline{2}$}<111>, and 24× {12$\underline{3}$}<111> slip systems. The center grain has Goss orientation, {011}<100>, and the surrounding grain has rotated cube orientation, {001}<110>. The gray scale quantifies the accumulated misorientation at each integration point (with light values indicating large misorientations). The figure shows that the two grains reveal very little interaction. The shape changes of both individual crystals follow the exerted plane strain deformation state. The texture changes in both individual crystals, given in {111} pole figures [Fig. 9(a)], are similar to those observed already in the corresponding single crystals [Fig. 6(a,c)]. This homogeneous plastic co-deformation of both grains can be attributed to two points which are known from grain interaction

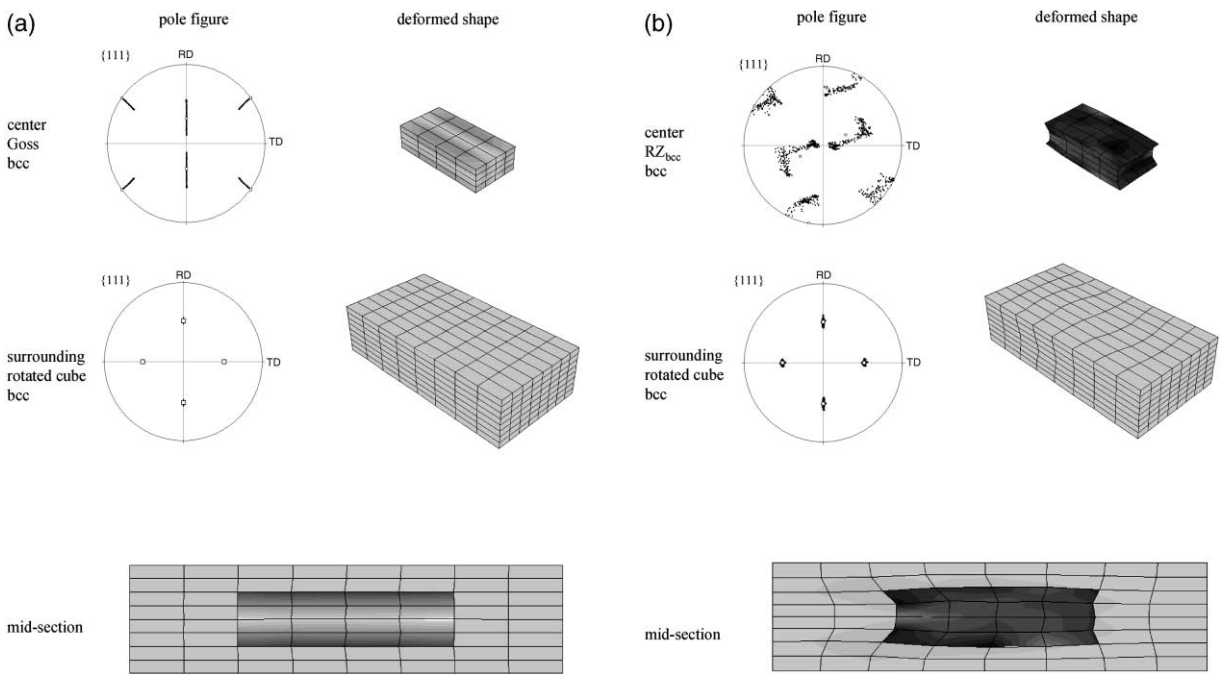

Fig. 9. (a) Example of a bcc bicrystal (48 slip systems), where the center grain has Goss orientation and the surrounding grain has 45° about normal rotated cube orientation. (b) Example of a bcc bicrystal (48 slip systems), where the center grain has RZ_{bcc} orientation and the surrounding grain has 45° about normal rotated cube orientation.

homogenization theory. First, both grains obviously have small shear tendency under plane strain deformation conditions. A grain is characterized by a large shear tendency when the required amount of shear on its slip systems (Taylor factor) can be lowered by dropping some of the external shape prescriptions at the cost of compatibility with the neighbor grains. Allowing for the partial relaxation of shear constraints means for orientations with large shear tendency that less slip is required for fulfilling the remaining non-relaxed constraints. Small shear tendency, as in Fig. 9(a), occurs when little or no deformation energy can be saved by dropping external constraints and shearing into a neighbor grain [57]. A second factor is that both grains reveal similar kinetic hardness, i.e. both individual crystals undergo nearly identical thickness reduction. It is an important fact that irrespective of the obvious strain and stress compatibility of the two grains the Goss crystal reveals the formation of strong orientation gradients.

Fig. 9(b) shows a different example of a bcc bicrystal. The center grain has RZ_{bcc} orientation and the surrounding grain has again {001}<110> orientation. In this case compatibility in shape change is not given among the two interacting crystals. The pole figures show that the interaction leads to a stronger orientation spread in the {001}<110> component when compared to the corresponding single crystal [Fig. 6(a,e)]. Table 1 summarizes some pole figures obtained from the bicrystal results for the bcc crystal structure. The data show the rotated cube ($\varphi_1 = 0°$, $\phi = 0°$, $\varphi_2 = 45°$) component, an orientation close to the rolling texture fiber ($\varphi_1 = 0°$, $\phi = 18°$, $\varphi_2 = 17°$), and the rotated Goss orientation ($\varphi_1 = 0°$, $\phi = 90°$, $\varphi_2 = 45°$) as surrounding grains and the inverse Brass component ($\varphi_1 = 0°$, $\phi = 35°$, $\varphi_2 = 45°$), another orientation close to the rolling texture fiber ($\varphi_1 = 0°$, $\phi = 18°$, $\varphi_2 = 73°$), the Goss orientation ($\varphi_1 = 0°$, $\phi = 45°$, $\varphi_2 = 0°$), and the RZ_{bcc} orientation ($\varphi_1 = 34°$, $\phi = 84°$, $\varphi_2 = 45°$) as center grains.

The textures show the influence of neighbor

Table 1
(a) Some pole figures obtained from 3D bicrystal finite element results for bcc crystal structure. The textures show the influence of neighbor interaction on the resulting orientation gradients for different bicrystal combinations. This table shows the pole figures for the center grains (see Figs. 8 and 9). (b) Some pole figures obtained from bicrystal finite element results for bcc crystal structure. The textures show the influence of neighbor interaction on the resulting orientation gradients for different bicrystal combinations. This table shows the pole figures for the surrounding grains (see Figs. 8 and 9)

(a)

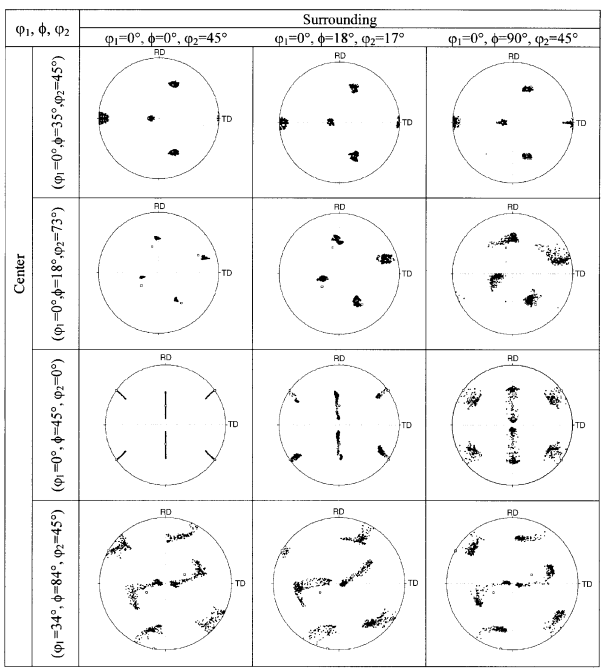

(b)

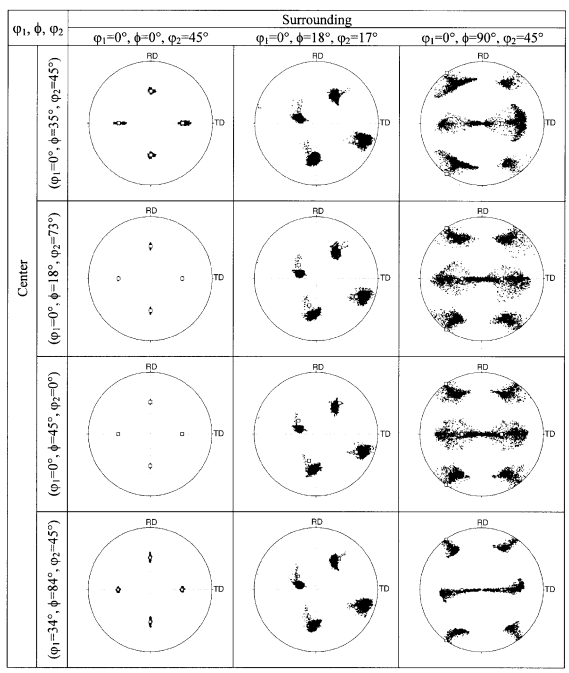

interaction on the resulting orientation gradients for different bicrystal combinations. Table 1(a) shows the pole figures for the center grains and Table 1(b) for the surrounding grains. Comparing these data with the pole figures given in Fig. 6 for the single grains[5] suggests that a significant dependence of the tendency to form orientation gradients on the neighbor crystals occurs particularly for grains with high positive divergence. Examples are the RZ_{bcc} orientation and the Goss orientation. Both texture components revealed very high divergence of their reorientation rate vector field [Fig. 3(a)]. The bicrystal finite element results confirm these predictions and show at the same time that their orientation spread depends considerably on changes in the neighbor orientations. The tendency to form orientation gradients within grains with close to zero or negative divergence reveals much smaller sensitivity to the orientation of the neighbor grain. For instance the Inverse Brass orientation [Table 1(a)] and the 45° rotated cube component [Table 1(b)] show less changes in the orientation spread when their neighbor grains are changed.

[5] The *single grains* (Figs. 6 and 7) have a constrained surface to preserve orthorhombic symmetry during straining. They must not be confused with *single crystals*.

4.3. Results for face centered cubic crystal structure (extrinsic, FEM)

Fig. 10(a) shows an example of a deformed bicrystal consisting of two grains with fcc crystal structure using 12× {11̲1}<110> slip systems. The center grain has RZ_{fcc} orientation and the surrounding grain has Goss orientation. The gray scale quantifies the accumulated misorientation at each integration point (light values indicate large misorientations). The figure shows that the two grains reveal very little plastic interaction, i.e. nearly no mutual distortion takes place and both individual crystals follow the external plane strain state. The texture changes in both individual crystals, given in {111} pole figures [Fig. 10(a)], are similar to those observed in the single crystals [Fig. 7(a,d)]. In the bicrystal arrangement the Goss orientation reveals a larger scatter than as a single crystal. In contrast, the RZ_{fcc} oriented center grain in the bicrystal reveals weaker orientation gradients than as a single crystal. Like in the bcc case this homogeneous co-deformation of the two grains can—when translated into homogenization theory—be understood in terms of their small shear tendency under plane strain deformation conditions and in terms of their similar Taylor factors.

Fig. 10(b) shows a different example of an fcc bicrystal. The center grain has Brass orientation and the surrounding grain has again Goss orientation. In this case the two interacting crystals do not preserve self-similar shapes as the couple in Fig. 10(a). Since the Goss orientation alone deforms symmetrically the strong shape distortion observed at the interface of the two grains can be attributed to the strong shear tendency of the Brass orientation. The two pole figures show that the interaction leads to a significantly stronger formation of orientation gradients in the Goss component when compared to the corresponding single crystal [Fig. 7(a)] and to the bicrystal in Fig. 10(a). In contrast, the orientation scatter in the deformed Brass orientation in the bicrystal is much smaller than in the corresponding single crystal [Fig. 7(b)].

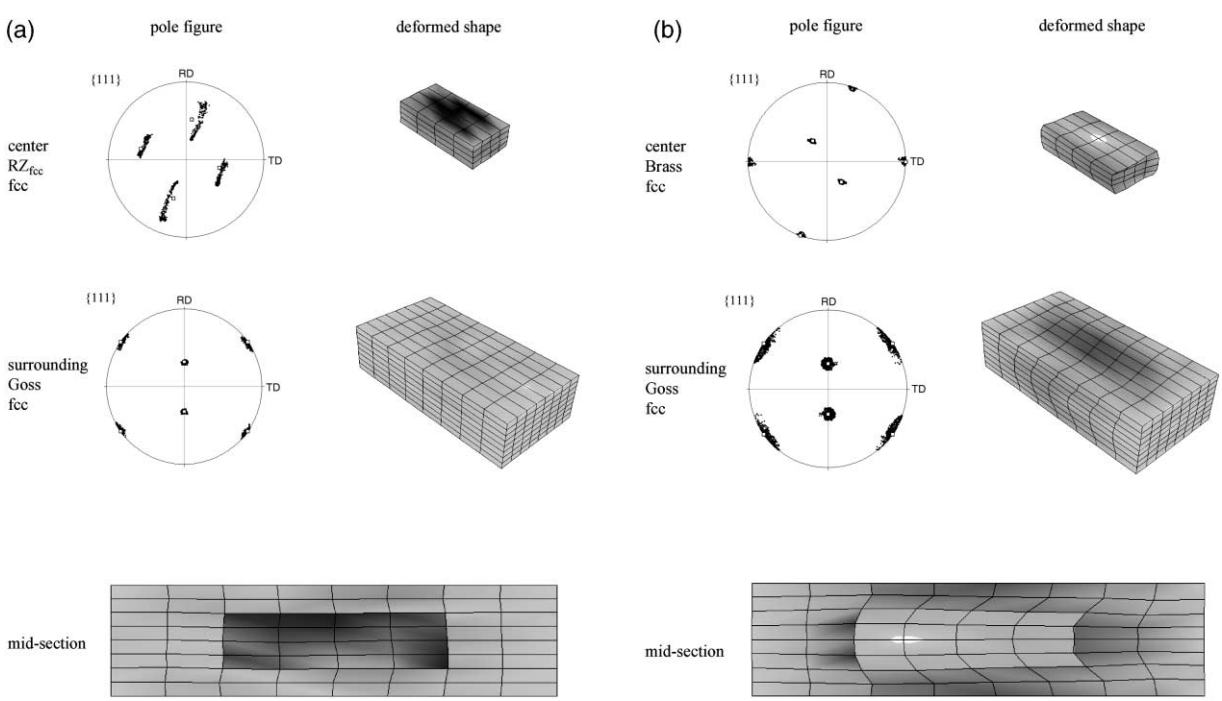

Fig. 10. (a) Example of an fcc bicrystal (12 slip systems), where the center grain has RZ_{fcc} orientation and the surrounding grain has Goss orientation. (b) Example of a bcc bicrystal (12 slip systems), where the center grain has Brass orientation and the surrounding grain has Goss orientation.

The simulations shows that a bicrystal where one grain has a much larger intrinsic tendency to form orientation gradients than the other one tends to distribute the overall orientation scatter over both crystals rather than concentrating it in one crystal (namely in the one which tends to form larger orientation gradients in the intrinsic case).

Beyond the examples given in Fig. 10(a,b) and Table 2 summarizes the pole figures of further fcc bicrystal arrangements. The data show the Goss orientation ($\varphi_1 = 0°$, $\phi = 45°$, $\varphi_2 = 0°$), the S orientation ($\varphi_1 = 60°$, $\phi = 32°$, $\varphi_2 = 65°$), and the rotated cube ($\varphi_1 = 45°$, $\phi = 0°$, $\varphi_2 = 0°$) component as surrounding grains and the Brass component ($\varphi_1 = 35°$, $\phi = 45°$, $\varphi_2 = 0°$), the Copper orientation ($\varphi_1 = 90°$, $\phi = 30°$, $\varphi_2 = 45°$), the cube component ($\varphi_1 = 0°$, $\phi = 0°$, $\varphi_2 = 0°$), and the RZ_{fcc} orientation ($\varphi_1 = 32°$, $\phi = 85°$, $\varphi_2 = 85°$) as center grains.

The textures show the influence of neighbor interaction on the resulting orientation gradients for different bicrystal combinations. Table 2(a) shows the pole figures for the center grains and Table 2(b) for the surrounding grains. The data suggest that both, orientations with positive and also with close-to-zero divergence reveal a significant dependence of their tendency to form in-grain orientation gradients on the neighbor crystals.

Table 2
(a) Some pole figures obtained from 3D bicrystal finite element results for fcc crystal structure. The textures show the influence of neighbor interaction on the resulting orientation gradients for different bicrystal combinations. This table shows the pole figures for the center grains (see Figs. 8 and 10). (b) Some pole figures obtained from bicrystal finite element results for fcc crystal structure. The textures show the influence of neighbor interaction on the resulting orientation gradients for different bicrystal combinations. This table shows the pole figures for the surrounding grains (see Figs. 8 and 10)

(a)

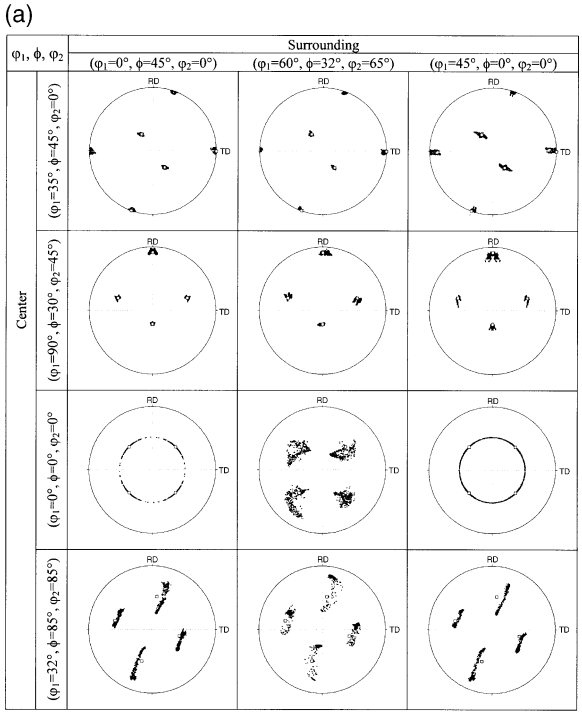

(b)

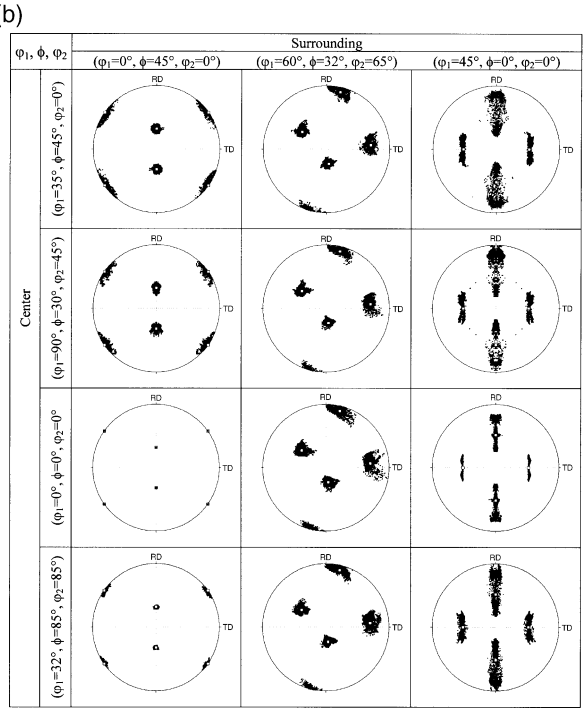

This is a different result than obtained for the bcc crystal structure [see Table 1(a,b)] which revealed less neighborhood dependence for crystals with small reorientation divergence. For instance the fcc Goss orientation and the fcc cube orientation turn out to show a strong dependence on the orientation of the neighbor grains (Fig. 10).

5. Discussion

Some of the presented predictions can be compared to experimental observations of orientation gradients in different texture components and crystal structures deformed under plane strain conditions. In case of the bcc crystal structure particularly the 45° rotated cube component, {001}<110>, is well known for its small in-grain orientation gradients even after large plane strain deformation. Particularly the EBSP (electron back scatter diffraction) method has provided detailed data about orientation gradients in this texture component. Raabe et al. reported that the orientation scatter in {001}<110> grains typically remains in the small angle grain boundary regime below 15° maximum in-grain misorientation (e.g. [3,30,31,33,58,62]). Similar observations for {001}<110> grains in polycrystalline specimens were made by Dillamore et al. [63,64]. Earlier work on that subject was conducted by Hu on deformed {001}<110> oriented iron–silicon single crystals [65,66]. Hu reported that {001}<110> oriented single crystals do not change their initial orientation during rolling deformation and reveal a uniform microstructure without orientation gradients after straining. From a simple though sufficiently realistic Schmid-type analysis Hu concluded that the slip systems activated for the plane strain deformation of a {001}<110> oriented grain are (101)[1$\bar{1}$1], (101)[$\bar{1}$11], (01$\bar{1}$)[$\bar{1}$11], (011)[1$\bar{1}$1]. These systems have little mutual elastic interaction and it is assumed that such conditions also promote weak strain hardening. The various experimental observations about in-grain orientation gradients in the rotated cube orientation are in excellent agreement with the predictions [Fig. 3(a,b), 6(a), 9(a,b)]. Particularly Fig. 9(a,b) and Table 1(b) demonstrate that the reluctance of this texture component against the formation of orientation gradients is not much affected by grain–neighbor interaction.

Apart from the rotated cube orientation which is in the bcc structure a good example for very weak orientation gradients stronger orientation scatter has been frequently found for {111}<uvw> and {112}<110> oriented grains (e.g. [30,31,33,58,67–72]). These studies reported that such grains reveal small cell sizes, high stored dislocation densities, and microstructural inhomogeneities such as shear bands which provide strong local misorientations. For the {111}<uvw> grains the correspondence between experiment and predictions is less well pronounced. Fig. 3(b) shows local maxima of the reorientation field divergence not exactly on the {111}<uvw> orientation fiber but in its immediate vicinity.

Another orientation which has been intensely investigated in the bcc structure is the Goss component, due to its importance in the fields of shear texture, recrystallization, and secondary recrystallization (e.g. [33,61,62,71,72]). It was essentially found that the Goss orientation is in the bcc lattice stabilized by shear strain. Under plane strain deformation it is not stable and splits up to rotate towards {001}<110> and {111}<112>, respectively, building up strong orientation gradients. The remaining transition zones between such orientation branches can preserve the Goss orientation and for instance provide later highly potential nucleation sites. The strong tendency of the Goss orientation to form such in-grain orientation gradients was correctly predicted both, by the divergence approach [Fig. 3(a)] and by the finite element approach [Fig. 6(c)].

Similar arguments as for the rotated cube orientation in the bcc lattice apply for the Goss component in the fcc lattice. Under ideal plane strain conditions it can essentially be deformed by four symmetric slip systems. Its small tendency to build up orientation gradients is not only found in the reorientation field divergence approach (Fig. 4, first section) but also in the single crystal simulations [Fig. 7(a)]. However, the fcc Goss component significantly differs from the bcc rotated cube orientation with respect to its stability under the influence of neighbor grains. Comparing Tables

1(b) (bcc) and 2(b) (fcc) shows that the fcc Goss orientation builds up larger in-grain orientation gradients when co-deformed with the Brass or the Copper texture components than the bcc rotated cube component. This difference which is also well known from experiment can be attributed to the fact that (in this investigation) the fcc orientations deform by use of 12 slip systems while the bcc orientations use 48 systems. In other words the bcc crystals have more degrees of freedom in the displacement and hence deform more like a continuum when compared to the fcc crystals. Bcc crystals can therefore obviously better accommodate changes in the local boundary conditions. This might also explain why the rotated cube orientation is in cold rolled bcc alloys typically much more pronounced relative to the other texture components (see typical bcc α- and γ-fibers) than the Goss orientation in the textures of cold rolled fcc alloys (see typical bcc α- and β-fibers).

Besides the complicated fcc Goss orientation also other fcc texture components have been well investigated with respect to orientation gradients. For instance many experiments confirm the present predictions of a relatively small tendency to build up pronounced orientation gradients in the fcc Brass orientation. In contrast the cube orientation and the S orientation were reported to form larger orientation gradients (e.g. [5–7,22–27,41, 48,73,74]). However, the present results for the Goss and the cube orientation underline that their deformation and rotation paths are in experiments more governed by their neighborhood rather than by their (rather weak theoretical) intrinsic tendency to form gradients.

The prediction and experimental observation of orientation gradients is not only a problem of fundamental interest in the field of crystal kinematics but is also important in the context of hardening and recrystallization. Although the fields of texture and dislocation theory have not yet been fully merged since the first works of Nye [8], Kröner [9], and Ashby [10] in this domain the occurrence of orientation gradients clearly implies the generation of corresponding in-grain populations of geometrically necessary dislocations. These may contribute in a statistical, mechanically equilibrated and thus scalar manner or even in a tensorial fashion to the overall hardening. In either context the present work suggests that in grains with a strong kinematical tendency to form in-grain orientation gradients the effect of geometrically necessary *hardening* should be taken into account. It can be anticipated that this will have a damping influence on the formation of orientation gradients since it provides a certain penalty term opposing further curvature. Vice versa this means that a theory of hardening—when considering geometrically necessary dislocations—must be formulated as an orientation dependent theory.

Similar arguments apply for the phenomenology of primary static recrystallization. It is a common observation that nucleation can only take place in areas with large stored elastic energy (thermodynamic instability criterion) and large orientation gradients (kinetic instability criterion). On the basis of the present approach the latter criterion implies that recrystallization nucleation must be considered as a highly orientation dependent problem (see e.g. [33]).

6. Conclusions

We introduced a theory of orientation gradients in plastically strained crystals. The aim was to explain why uniform crystals can—under gradient-free external loadings—build up in-grain orientation gradients during straining and how this phenomenon depends on the crystal orientation (intrinsic dependence) and on the neighbor grains (extrinsic dependence). The intrinsic origin of orientation gradients was explained in terms of the dependence of the crystal reorientation rate vector on variations in initial orientation. The dependence was quantitatively formulated by applying a divergence operator to reorientation rate vector fields calculated by strain-rate homogenization theory. The predictions were confirmed by crystal plasticity finite element simulations. The extrinsic influence on in-grain orientation gradients was addressed by investigating the effects of grain–neighbor interaction on the subdivision of crystals using a crystal plasticity finite element bicrystal model. The main conclusions are:

1. Orientation dependence of orientation gradients (intrinsic dependence)

   The *divergence* of reorientation rate vector fields can be used to quantify the intrinsic tendency for the formation of in-grain orientation gradients as a function of crystal orientation and strain state. The divergence analysis method is independent on the underlying deformation model or experiment. Its starting point can be any theoretical or experimental reorientation field in orientation space. The method makes no prediction about the spatial arrangement of orientation gradients. Positive divergence indicates orientations with diverging non-zero reorientation rates which are unstable and form orientation gradients. Zero divergence indicates orientations with reorientation rate identity with the surrounding orientations which are not prone to form orientation gradients. Negative divergence indicates orientations with converging non-zero reorientation rates which are kinematically stable and not prone to form orientation gradients. Intrinsic results on orientation gradients obtained by use of a crystal plasticity finite element formulation are in very good agreement with the reorientation field divergence function derived by homogenization theory. The predictions are in good accord with experiments except for the fcc Goss and the fcc cube orientation which reveal a high dependence of grain neighbor interaction.
2. Grain neighborhood dependence of orientation gradients (extrinsic dependence)

   Significant dependence of in-grain orientation gradients on the neighbor crystals (beyond their *intrinsic* tendency to form orientation gradients) was found in the bcc case for grains with high positive divergence and for the fcc case for grains with small and high positive divergence. The differences between bcc and fcc are due to the difference in slip selection (we used 12 systems for fcc and 48 for bcc). The formation of orientation gradients in crystals with close to zero or negative divergence depends less strongly on changes in the neighbor orientations. Exceptions occur for the fcc case where the Goss and the cube orientation reveal a strong dependence on grain neighborhood.

References

[1] Barrett CS, Levenson LH. Trans Metall Soc AIME 1940;137:112.
[2] Beaudoin AJ, Mecking H, Kocks UF. Phil Mag A 1996;73:1503.
[3] Raabe D. Phys Stat Sol (B) 1994;181:291.
[4] Leffers T. Int J Plastic 2001;17:469.
[5] Lee CS, Duggan DJ. Acta Metall 1993;41:2691.
[6] Lee CS, Duggan DJ, Smallman RE. Acta Metall 1993;41:2265.
[7] Ørsund R, Hjelen J, Nes E. Scripta Metall 1989;23:1193.
[8] Nye JF. Acta Metall 1953;1:153.
[9] Kröner E. Continuum theory of dislocations and internal stresses [in German]. New York: Springer Verlag, 1958.
[10] Ashby MF. Phil Mag 1970;21:399.
[11] Dillamore IL, Katoh H. Met Sci 1974;13:73.
[12] Becker R, Panchanadeeswaran S. Acta Metall 1995;43:2701.
[13] Becker R. Acta Mater 1998;46:1385.
[14] Becker R, Butter JF, Hu H, Lalli L. Met Trans A 1991;22:45.
[15] Becker R. Model Simul Mater Sci Eng 1995;3:417.
[16] Mika DP, Dawson PR. Acta Mater 1999;47:1355.
[17] Sarma GB, Dawson PR. Acta Mater 1937;1996:44.
[18] Dawson PR, Boyce D, MacEwen S, Rogge R. In: Szpunar JA editor. Proceedings of the 12th International Conference on Textures of Materials ICOTOM 12, Aug. 9–13, 1999, vol. 1. Ottowa: NRC Research Press; 1999:505.
[19] Raabe D, Becker R. Modelling Simul Mater Sci Eng 2000;8:445.
[20] Buchheit TE, Bourcier RJ, Wellman GW, Neilsen MK. Model Simul Mater Sci Eng 1997;5:421.
[21] Battaile CC, Buchheit TE, Holm EA, Wellman GW, Neilsen MK. In: Bulatov V, Diaz de la Rubia T, Ghoniem N, Kaxiras T, Phillips R, editors. Multiscale modeling of materials, MRS Symposium J, Boston, 1998.
[22] Akef A, Driver JH. Mater Sci Eng A 1991;132:245.
[23] Basson F, Driver JH. Acta Mater 2000;48:2101.
[24] Hughes DA, Hansen N. Acta Mater 1997;45:3871.
[25] Hjelen J, Weiland H, Butler J, Liu J, Hu WH, Nes E. Textures Microstruct 1991;14–18:983.
[26] Hjelen J, Ørsund R, Nes E. Acta Metall 1991;39:1377.
[27] Weiland H. Acta Metall 1992;40:1083.
[28] Engler O, Gottstein G. Steel Res 1992;63:413.
[29] Adams BL, Wright SI, Kunze K. Metall Trans A 1993;24:819.
[30] Raabe D, Boeslau J. In: Andersen SI, Bilde-Sorensen JB, Lorentzen T, Pedersen OB, Sorensen NJ, editors. Proceedings of the 15th RISØ International Symposium on Materials Science: Numerical Predictions of Def. Proceed-

ings and the Behaviour of Real Materials, Roskilde (Denmark): RISØ National Laboratory; 1994:481.
[31] Boeslau J, Raabe D. Mater Sci Forum 1994;157–162:501.
[32] Driver JH, Juul Jensen D, Hansen N. Acta Metall 1994;42:3105.
[33] Raabe D. Steel Res 1995;66:222.
[34] Bayer F, Fischer-Bühner J, Gottstein G. Intermetallics 1999;7:467.
[35] Weiland H, Field DP, Adams DP. In: Liang Z, Zuo L, Chu Y, editors. Proceedings of the 11th International Conference on textures of materials, Xi'ian (China). Beijing: International Academic Publishers; 1996. p. 141-4.
[36] Liu Q, Maurice C, Driver JH, Hansen N. Metall Mater Trans A 1998;29:2333.
[37] Weiland H. JOM 1994;46:37.
[38] Weiland H, Becker R. In: Leffers T, Pederson OP, editors. Proceedings of the 20th RISØ International Symposium on Materials Science: Deformation-induced Microstructures: Analysis and Relation to Properties, Roskilde (Denmark): RISØ International Laboratory; 1999:213.
[39] Krieger-Lassen NC, Jensen DJ. Mater Sci Forum 1993;113–115:679.
[40] Schwarzer R, Weiland H. In: Proceedings of the 7th International Conference on Textures of Materials, Amsterdam (North Holland); 1984:839.
[41] Hughes DA, Liu Q, Chrzan D, Hansen N. Acta Mater 1997;45:105.
[42] Zaefferer S, Schwarzer R. Z Metallk 1994;85:585.
[43] Zaefferer S. J Appl Cryst 2000;33:10.
[44] Zaefferer S, Schwarzer R. Proceedings of the 10th International Conference on Textures of Materials. Mater Sci Forum 1994;157–162:247.
[45] Zaefferer S. Proc Microsc Microanal 1999;99:202.
[46] Field D, Weiland H. Mater Sci Forum 1994;157–162:1181.
[47] Hughes DA. Proceedings 16th Int. RISØ Symposium on Materials Science, Roskilde (Dänemark), 1995, p. 63.
[48] Hughes DA, Kumar A. In: Liang Z, Zuo L, Chu Y, editors. Proceedings of the 11th International Conference on textures of materials, Xi'ian (China). Beijing: International Academic Publishers; 1996. p. 134-5.
[49] Kocks UF, Embury JD, Cotton JD, Chen SR, Beaudoin AJ, Wright SI, Rollett AD. In: Advances in hot deformation textures and microstructures. Warrendale (PA): The Metallurgical Society of AIME; 1994:459.
[50] Bunge HJ. In: Bunge HJ, Esling C, editors. Theoretical methods of texture analysis. Frankfurt: DGM Informationsgesellschaft, Deutsche Gesellschaft für Metallkunde, 1987, p. 407.
[51] Klein H, Dahlem E, Esling C, Bunge HJ. In: Bunge HJ, Esling C, editors. Theoretical methods of texture analysis. Frankfurt: DGM Informationsgesellschaft, Deutsche Gesellschaft für Metallkunde, 1987, p. 259.
[52] Seefeldt M, Delannay L, Peeters B, Aernoudt E, Van Houtte P. Acta Mater, in press.
[53] Delannay L. Ph.D. dissertation, May 2001, Katholieke Universiteit Leuven, Belgium.
[54] Roters F, Raabe D. In: Raabe D, Bunge HJ, editors. Proceedings of the Symposium Computer Simulation and Modelling in Texture Research, Aachen, October 13–14, 1995, Special Edition of Textures and Microstructures. London: Gordon and Breach; 1997:167.
[55] Aernoudt E, van Houtte P, Leffers T. In: Mughrabi H editor. Deformation and txtures of metals at large strains, materials science and technology—a comprehensive treatment, vol. 6. Weinheim: VCH; 1993:89.
[56] Kocks UF, Tomé CN, Wenk H-R. Texture and anistropy. Cambridge: Cambridge University Press, 1998.
[57] Raabe D. Computational materials science. Weinheim: Wiley-VCH, 1998.
[58] Raabe D, Schlenkert G, Weisshaupt H, Lücke K. Mater Sci Technol 1994;10:229.
[59] ABAQUS/standard user's manual, vol. II, 14.1.4-1. Pawtucket (RI): Hibbitt, Karlsson and Sorensen, 1999.
[60] Kalidindi SR, Bronkhorst CA, Anand L. J Mech Phys Solids 1992;40:537.
[61] Hölscher M, Raabe D, Lücke K. Acta Metall 1994;42:879.
[62] Raabe D, Lücke K. Scripta Metall 1992;27:1533.
[63] Dillamore IL, Morris PL, Smith CJE, Hutchinson WB. Proc R Soc A 1972;329:405.
[64] Dillamore IL. In: Haessner F, editor. Recrystallization of metallic materials. Stuttgart: Dr Riederer Verlag GmbH; 1984:223.
[65] Hu H. Trans AIME 1962;224:75.
[66] Hu H. In: Himmel L, editor. Recovery and recrystallization of metals. New York: Wiley and Sons; 1963:311.
[67] Dillamore IL, Smith CJE, Watson TW. Met Sci J 1967;1:49.
[68] Hutchinson WB. Acta Metall 1989;37:1047.
[69] Inokuti Y, Doherty R. Acta Metall 1978;26:61.
[70] Ushioda K, Hutchinson WB, Agren J, von Schlippenbach U. Mater Sci Technol 1986;2:807.
[71] Raabe D, Lücke K. Mater Sci Forum 1994;157–162:597.
[72] Hölscher M, Raabe D, Lücke K. Steel Res 1991;62:567.
[73] Wassermann G, Grewen J. Texturen metallischer Werkstoffe. Berlin: Springer Verlag, 1962.
[74] Delannay L, Mishin OV, Juul Jensen D, Van Houtte P. Acta Mater 2001;49:2441.